

Urban source term estimation for mercury using a boundary-layer budget method

Basil Denzler¹, Christian Bogdal¹, Cyrill Kern¹, Anna Tobler^{1,2}, Jing Huo¹, and Konrad Hungerbühler¹

¹Institute for Chemical and Bioengineering, ETH Zurich, Vladimir-Prelog-Weg 1, CH-8093 Zurich, Switzerland

²present address: Paul Scherrer Institute, CH-5232 Villigen PSI, Switzerland

Correspondence: Christian Bogdal (christian.bogdal@chem.ethz.ch)

Abstract. Mercury is a heavy metal of particular concern due to its adverse effects on the human health and the environment. Recognizing this problem, the UN Minamata Convention on Mercury was recently adopted, where signatory countries agreed to reduce anthropogenic mercury emissions. To evaluate the effectiveness of the convention, quantitative knowledge on mercury emissions is crucial. So far, bottom-up approaches have successfully been applied to quantify mercury emission – especially for point sources. Distributed sources make up for a large share of the emission, however, they are still poorly characterized. Here, we present a top-down approach to estimate mercury emissions based on atmospheric measurements in the city of Zurich, Switzerland. While monitoring the atmospheric mercury concentrations during inversion periods in Zurich, we were able to relate the concentration increase to the mercury emission strength of the city using a box model. By the means of this boundary-layer budget approach, we succeeded to narrow down the emissions of Zurich to range between 41 ± 8 kg/a (upper bound) and 24 ± 8 kg/a (lower bound). Thereby, we could quantify emissions from mixed, diffuse and point like sources and derive an annual mercury per capita emission of 0.06 to 0.10 g/a. The approach presented here has the potential to support authorities in setting up inventories and to validate emission estimations derived from the commonly applied bottom-up approaches. Furthermore, our method is applicable to other compounds and to a wide range of cities or other areas, where sources or as well sinks for mercury and other atmospheric pollutants are presumed.

15 *Copyright statement.* TEXT

1 Introduction

The UN Minamata Convention on Mercury entered into force in August 2017. It marks a milestone in the ambitions of the global community to protect the human health and the environment from the adverse effects of mercury and mercury compounds. The parties to this convention have agreed to control mercury emissions and establish an inventory of emissions from relevant sources. Furthermore, the convention recognizes the need for research and monitoring to increase the state of knowledge regarding the emission and distribution pathways of mercury. Numerous measurement campaigns for atmospheric mercury have been conducted worldwide. [They show gaseous elemental mercury \(GEM\) concentration with more 90% to be](#)

the dominant atmospheric mercury species, while gaseous oxidized mercury (GOM) and particle bound mercury (PBM) make up for small share in background air (Gay et al., 2013).

The tools applied in the analysis of these measurement results encompass among others: wind rose interpretations, back trajectories and various statistical analysis. Potential sources for mercury can thereby be located but a quantification of their emission strength is not achieved. For testing the effectiveness of an international treaty such as the Minamata convention, however, quantitative information on emission and changes thereof are crucial. This task of assessing the sources is often left to authorities which follow the guidelines for the bottom-up approach AMAP/UNEP (2013). The inventories established with this method are very valuable and so far certainly provide the best and most reliable emission estimates. However, these inventories address emission usually on a national level and focus heavily on large point sources. Additionally, the apportionment of total national emissions to regional emissions is a difficult task, requiring various assumptions. To obtain spatially resolved emissions two steps are applied. First, mercury emissions are assigned to point sources where possible. And second, so called 'distributed sources', that make up for >80% of total emissions worldwide, are mapped using a surrogate on the basis of population density data (Wilson et al., 2006; AMAP/UNEP, 2013). Top-down studies confirming the allocation praxis of distributed mercury emissions in bottom-up inventories are lacking. For scientific requirements, verification and testing of these inventories with other independent methods is necessary, as has similarly been suggested for greenhouse gases (Nisbet and Weiss, 2010). In this work, we present a top-down method that allows quantification of mercury emissions in an urban environment. The goal is to support authorities with the interpretation of their valuable and expensive monitoring studies and and to ultimately introduce a top-down method that could help to verify and refine mercury emission inventories regarding distributed emissions. To achieve this refinement, the method has to be applicable to numerous locations worldwide with limited resources. For our model set-up we make use of the meteorological phenomenon of a ground inversion. The reduced vertical mixing during high-pressure winter periods or summer nights above ground leads to an accumulation of atmospheric pollutants below the boundary air layer. Inversion effects occur frequently in metropolitan areas all over the world, such as: Los Angeles, Beijing, Milan, Mexico City, Teheran or Mumbai and can lead to adverse effects for the population. In such locations, a boundary-layer budget method (Denmead et al., 1996) can be applied during inversion events to estimate the source strength of these substances, since it is then proportional to their concentration increase. We apply this approach to the city of Zurich, Switzerland, which serves as a representative site for Switzerland, which is in turn representative for an industrialized country in Europe with existing mercury regulation and is also party to the Minamata convention. Additionally, we can profit from our previous studies, where our model has been extensively validated for the city of Zurich and the top-down approach could successfully be applied to quantify emissions of various anthropogenic pollutants. Our previous studies reported top-down derived emissions in Zurich for industrial chemicals, including polychlorinated biphenyls (PCB) (Gasic et al., 2009; Bogdal et al., 2014a; Diefenbacher et al., 2016), flame retardants (Bogdal et al., 2014b; Diefenbacher et al., 2015a), perfluorinated surfactants (Müller et al., 2012; Wang et al., 2012) unintentional combustion byproducts, including polychlorinated dibenzo-p-dioxins and dibenzofurans (Bogdal et al., 2014a), or additives of personal care products such as cyclic methylsiloxanes (Buser et al., 2013). Furthermore, this method is not only applicable to Zurich, but to a multitude of locations and has successfully been applied to various substances as for example PCBs in Chicago, USA, Hazelrigg, UK, Finokalia, Greece, Banja Luka,

Bosnia and Hercegovina (MacLeod et al., 2007; Gasic et al., 2010), cyclic methylsiloxanes in Chicaco, USA (Buser et al., 2014), chloro- and hydrofluorocarbon propellants nearby Zurich, Switzerland (Buchmann et al., 2003), methane in London, UK (Lowry et al., 2001) and St. Petersburg, Russia (Zinchenko et al., 2002). Wherever smog problems arise such a boundary-layer budget is technically feasible. We hypothesize that mercury has relatively constant emissions and follows the pattern of accumulation during strong inversion periods similarly to the organic pollutants cited before. By developing and applying a box-model for the city of Zurich our aim is to derive the emission source strength of Zurich. Furthermore, we extrapolate our findings to whole Switzerland and compare the calculated emissions to reported emissions from bottom-up inventories. Finally, we discuss the applicability of our boundary-layer budget approach in a general context.

2 Measurements and Methods

2.1 Measurements

Gaseous elemental mercury (GEM) concentrations have been measured from December 2013 until December 2015 at the sampling station of the Swiss National Air Pollution Monitoring Network (NABEL), Zurich Kaserne, Switzerland. It is located in a large courtyard (approximately 9000 m²) in the city center of Zurich (47.38°N, 8.53°E, 409 m above sea level) shielded from highly frequented roads and industrial activities. Since decades, the site has provided continuous monitoring of the major air pollutants and a multitude of meteorological parameters, such as the wind speed, used in this study as a model parameter. Previous work on particulate matter (PM-10) (Hasenfratz et al., 2015; Mueller et al., 2016), nitrogen oxides (NO_x) (Mueller et al., 2015) and persistent organic pollutants (Bogdal et al., 2014a; Diefenbacher et al., 2015b, 2016) have shown that the measurement location provides representative background levels for the city of Zurich and is not affected by acute emissions close to the site. For GEM measurements air was sampled through an inlet and analyzed using a Tekran[®] 2537X cold vapor mercury analyzer with a detection limit lower than 0.1 ng/m³ stated by the manufacturer. Flow rate was 1.5 l/min and measurements were taken every 5 minutes from alternating cartridges. The instrument was automatically calibrated every 25 hours. Additionally, manual calibrations of the permeation source were performed using an external calibration device (Tekran[®] 2505) and comparison measurements were conducted with an instrument identical in construction to ensure data quality. Furthermore, GEM was measured during a single monitoring campaign (January - February 2016) using the same measurement device on a cite in the periphery of Zurich (Zurich Zoo, 47.38°N, 8.58°E, 587 m above sea level), to obtain indications for the background influx of air in Zurich. Methane (CH₄) and carbon monoxide (CO) measurements were provided by NABEL (BAFU; EMPA, 2018). CH₄ levels are used as a conservative trace gas to compare to GEM levels, while CO is used as combustion indicator.

2.2 Model design

For the model design, we take advantage of the meteorological conditions of a temperature inversion that can occur during high-pressure periods. A phenomenon where – due to the faster cooling of the earth surface – the temperature profile in the

atmosphere becomes inverted. Higher in density, cold air resides at the surface and temperature increases with height until the boundary-layer [top](#) is reached. This leads to a stratification of air masses, where vertical mixing is very low. In Zurich this phenomenon is enhanced by the valley topography, where cold air drains into the depression. The reduced convective mass transfer to the warmer air masses above thus restricts the air volume in direct contact with the surface. In summer this phenomenon usually only occurs during the night. The strong soil heating and the resulting thermal lift break up the inversion soon after daybreak. In winter, with lower sun intensity, inversion conditions can prevail for several days up to weeks leading to the well known smog problematic. With steady emissions at the ground level into the smaller volume of the surface layer, an increase in concentration for air pollutants is observable (Salmond, 2005; MacLeod et al., 2007). This not only accounts for commonly monitored air pollutants such as CH₄, CO, NO_x, volatil organic compounds (VOCs) and aerosols such as PM-10, but as well for trace chemicals of anthropogenic origin such as persistent organic pollutants (Gasic et al., 2009; Müller et al., 2012; Wang et al., 2012; Bogdal et al., 2014a, b; Diefenbacher et al., 2015a, b), cyclic methylsiloxanes (Buser et al., 2013) or chloro- and hydrofluorocarbons (Buchmann et al., 2003). Under the assumption of constant emissions, the slope of the increase in concentrations is proportional to the emission flux. By setting-up a box model, we make use of this circumstance and are able to derive the emission term for the investigated air pollutant. This approach is thereafter also referred to as boundary-layer budget.

15

2.3 Model parametrization

Over the course of the measurement period nine episodes of day-night inversion were identified by visual inspection ~~of the data for the criteria of strong day/night inversion~~. Only events lasting for a minimum of four days were considered. Individual periods show a considerably longer duration of up to 14 days. These events are then reproduced with our previously developed and validated model ~~model~~. While in our previous studies, the temporal resolution of the air monitoring was significantly limited (resolution of hours to weeks), we profit here from highly resolved GEM data (5 min resolution). We follow the approach to strip the model to the minimum, only processes indispensable to parametrize the conditions at hand are incorporated. This lean model approach prevents over interpretation of model results and the reduced complexity provides a better conceivability of the model. Thereby, we end up with a model consisting of a single box of air that covers an area A , of 10 km × 10 km (100 km²) approximating Zurich's size inhabited by roughly 400'000 people (Fig. 1). The box size was chosen such as to encompass the city's emission sources and has proven to be suitable by previous studies (Wang et al., 2012; Buser et al., 2013; Bogdal et al., 2014b). Based on the national emission inventory (Heldstab et al., 2015) half the mercury emissions are assumed to stem from mixed sources such as stationary combustion, minor industrial activities and houses distributed all over the city. The other halve comes from a [municipal](#) waste incineration plant in the middle of the city, where a chimney (height 90 m) leads to a broader distribution. For Zurich this shows an emission profile similar to unintentional combustion byproducts such as polychlorinated dibenzo-p-dioxins and dibenzofurans studied in the work of Bogdal et al. (2014b). ~~Therefore GEM concentrations can be assumed to be homogeneously mixed~~ Since for this study on GEM, we only have one measurement location at near surface level, the assumption of a homogeneously mixed air compartment below nocturnal BL is necessary. The previous work on dioxins have shown that this assumption is justifiable. Possible stratification, however, remains a source for uncertainty to

our model. Emissions of oxidized mercury species such as HgCl_2 as well as particulate mercury were not included in the model compartment. Regarding the local emissions of oxidized mercury we did not have any data available. The only major source would be the municipal waste incineration plant. Considering the flue-gas treatment systems installed, however, we assume stack emissions to be predominantly in the form of GEM (van Velzen et al., 2002). Flue-gas is treated with ESP, SCR, AC, and 3-step WFGD in this order. (ESP: electrostatic precipitator, SCR: selective catalytic reduction, AC: activated carbon injection, WFGD: wet flue-gas desulfurization). Regarding the GEM/GOM ratio the effect of flue-gas treatment on mercury emissions is, however, still unclear leaving some level of uncertainty to our assumption (Zhang et al., 2016). Mercury emissions stemming from reduction of oxidized mercury reservoirs are thus contained in the total GEM emission estimates.

The time dependent parameters included in the model are: i) the boundary-layer height (BLH), defining the volume of the box ii) the wind speed to model advective flux (F) through the box and iii) the background concentrations to quantify the concentrations of the advective flux.

The model is operated dynamically with an hourly resolution. Due to the ~~relatively short periods of maximum 14 days simulated with our model~~, small size of the model area, many parameters usually included in box models can be disregarded. Slow processes such as deposition to soil and water, as well as re-emission from these compartments ~~and atmospheric degradation are excluded~~ are negligible. Atmospheric oxidation of GEM to GOM is excluded as well due to the short residence time of mercury within the considered small model region (less than 1 hour for wind speed of 3 m/s). Our own calculations, with a version including atmospheric degradation reactions, show that losses by degradation are negligible in comparison to the advective fluxes.

The focus of the model is on the emission flux, which is directed to the surface air compartment and is kept constant over the course of an inversion ~~period~~ period. The goal is to find the emission term that results in a modeled surface GEM concentration matching best the measured concentrations. The emission flux is the only adjustable parameter in the model, whereas all further model parameters are pre-set and not adapted to improve the fit between model results and field measurements. The residual mean square error (RMSE) is used as a measure for optimization in an iterative fitting process. The emission flux resulting in the lowest RMSE is then applied as the city's source term.

2.3.1 Model set-up

The model includes the following three time dependent model parameters.

(i) **The boundary-layer height (BLH)** is used as a measure to define the volumes of the air compartment of the model (Fig. 1). In a first model approach boundary-layer heights are approximated using constant levels for the daylight and nightly period. The height is set to 1500 m for the convective boundary-layer (CBL) during the day from 8 a.m. (UTC+1) until 8 p.m. and lowered to 150 m for the nocturnal boundary-layer (NBL) at 9 p.m.. The NBL level is based on common meteorological conditions (Stull, 1988) and our own experiences of previous work (MacLeod et al., 2007; Gasic et al., 2009; Wang et al., 2012; Buser et al., 2013; Bogdal et al., 2014b). A sharp transition is used between NBL and CBL. These heights determine the box volume of the air layer. Changes in volume of the air compartment are handled such that in case of a decline in BLH, the amount of GEM in the volume difference is transferred out of the box. In case of a rise of the BLH, the GEM concentration in

the air compartment is diluted with the corresponding air volume with GEM concentration of background levels.

(ii) **The advection** is determined by the wind speed. Wind speed measurements are conducted above a roof top (33 m.a.g.l.). Work by Benz (1988); Schuhmacher (1992) in Zurich show that measurements at this height are representative for the mean
5 wind speed for the height profile from 0 - 150 m. As shown later only nightly periods where the BLH is 150 m are relevant to estimate emissions in Zurich. Wind direction is not taken into consideration. Therefore, advection F is always occurring through a lateral face of the box (Fig. 1) and the flux is obtained by multiplication of its area A_s with the corresponding wind speed u , $F = A_s \cdot u$.

(iii) **The background concentration** is set to a steady level of 1.5 ng/m^3 . It lies in the lower 10% quantile of the whole two
10 year measurement series in Zurich and no adaption was made for nightly backgrounds. In reality background concentrations are likely to be higher than this level since also at high wind speeds measurements rarely fall below as we show in Fig. S1 and S2. The value of 1.5 ng/m^3 lies in the range of what we measured at outskirts of the city of Zurich (Zurich Zoo, median = 1.62 ng/m^3 , $Q_{0.1} = 1.53 \text{ ng/m}^3$, $Q_{0.9} = 1.77 \text{ ng/m}^3$). On the basis of these assumption an upper bound model run regarding
15 the source strength of the city is calculated. To establish a margin, which restricts the source strength with a realistic lower bound, background concentration are raised to the median concentration of 1.8 ng/m^3 for a second emission estimate. We are confident that actual emissions reside within the range of these two model runs.

3 Results and discussion

3.1 Measurement series

20 GEM levels measured in Zurich from December 2013 until December 2015, show a median concentration of 1.81 ng/m^3 ($Q_{0.1} = 1.55 \text{ ng/m}^3$, $Q_{0.9} = 2.36 \text{ ng/m}^3$). The concentration gradient for GEM follows a weak diurnal pattern, similar to CH_4 concentrations, however, with a more prominent amplitude. Figure 2 shows the diurnal pattern of GEM, CH_4 (i.e. conservative tracer), and CO (i.e. combustion indicator) measurements normalized by their respective mean concentration. The rise
25 in concentrations during night-time and the minimal concentrations during the afternoon are anti-cyclical to the wind speed and suggest a meteorological cause for the pattern. Stable conditions with lower wind speeds and lower boundary layer height during the night lead to a slight concentrations rise, while higher thermal convection during day-time lower these concentrations. The wind rose plots (Fig. S3) for GEM, CH_4 and CO support these findings and our initial hypothesis of a constant source term of GEM for the city. GEM concentrations are thus primarily influenced by the wind speed and the diluting effect of lower background concentrations (Fig. S2). However, one can observe as well slightly lower GEM concentration towards
30 the weekend with the lowest concentrations on Sundays (Fig. 2). More prominently this is the case for CO, which has sources that are strongly activity related, such as traffic. We therefore deduce that besides the prominent constant sources for GEM, there are as well activity related emissions, but of much smaller scale. The inversion events for the summer extracted from the measurement series show a clear diurnal trend not only for GEM but also for CH_4 (Fig. S4), both trace gases stem from

constant sources. In winter inversion periods also concentrations for PM-10, CO, SO₂, NO_x follow the course of GEM since combustion related sources have a more constant source term (Fig. S5). These comparisons indicate that the emission flux for GEM and CH₄ are constant over time.

5 For the measurement series at Zurich Zoo on the outskirts of the city a median GEM concentration of 1.62 ng/m³ (Q_{0.1} = 1.53 ng/m³, Q_{0.9} = 1.77 ng/m³) was obtained. GEM levels are significantly lower and the concentration range is much smaller at this measurement site. A clear indicator that this location is much less affected by local sources. Furthermore, these results confirm the assumption that background air is lower in concentration and suggest that background concentrations at a level of 1.5 ng/m³ are in fact a lower bound estimate.

3.2 Boundary layer budget

10 To illustrate the model results, we present the period showing longest continuing day-night inversion from 24 June until 06 July 2015 (Fig. 3) as an example. Analogous figures for the other eight inversion periods are shown in the Supplement (Fig. S6-S14). The figure shows the most important model parameters: the boundary-layer height (Fig. 3a), the wind speed (Fig. 3b), and Fig. 3c the measured GEM concentrations (blue), as well as the model results (red). GEM measurements show a clear diurnal variation with high concentrations of up to more than 3 ng/m³ during the night and lower concentrations during the day. The model results follow this pattern. The emissions strength of the city is observable from the steep concentration increase, when the BLH is lowered. These nocturnal periods with low wind speeds (< 2 m/s) are used to estimate the source term of the city. During daytime the modeled concentrations are dominated almost entirely by the background concentrations due to the higher BLH and the stronger wind speeds, which create a much bigger flux than the city's GEM emissions.

15 In general, model results follow the measured concentration suggesting advection and boundary-layer height are indeed enough to describe most of the GEM variation. During day-time model results are slightly lower than measured GEM levels, showing that our model approach covers the most important atmospheric processes occurring on this time scale and successfully reproduce the fate of GEM in the urban air of Zurich. By RMSE reduction we find a GEM emission flux of 4.8 g/hour (Table 1) for the modeled region in this period, or 42 kg/a when extrapolated to annual emissions for the city of Zurich. Over all nine periods, we find a mean emission of 4.7±0.9 g/hour or 41±8 kg/a (Table 1). The low variance of the emission estimate over all 20 the nine periods from different months and years supports our claim of a constant mercury emission term for the city. Also for three winter periods with long stable inversion conditions (Fig. S15-S17) emission estimates in the same range are observed (4.4±0.8 g/hour, see Table S1).

3.2.1 Uncertainties of the emission estimates

The mass balance for mercury in the air compartment of the box (m) formulates as follows:

$$30 \quad \frac{dm}{dt} = V \cdot \frac{dc}{dt} = F_{adv} \cdot c_{back} - F_{adv} \cdot c(t) + E \quad (1)$$

$$\frac{dm}{dt} = u \cdot A_s \cdot c_{back} - u \cdot A_s \cdot c(t) + E \quad (2)$$

where V [m^3] is the Volume of the box, c_{back} is the background concentration [ng/m^3], E is the emission flux [g/s]. The advective air flux F_{adv} [m^3/s] is calculated from the wind with velocity u [m/s] that flows through the lateral side of the box A_s [m^2]. Although the emission estimations presented so far are based on a dynamic time-resolved box model, we introduce here the steady state case for sake of simplification. For the steady state solution ($\frac{dm}{dt} = 0$) the emission flux is $E = u \cdot A_s \cdot (c - c_{\text{back}})$.

5 The problem at hand are of linear nature. Therefore, error handling is straightforward and maximum error bound could be found using linear error propagation (MacLeod et al., 2002) and a given uncertainty in a parameter would at worst results in an equal uncertainty in the model result. However, the true errors of the parameters are unknown and not all of them would strictly follow a known distribution. The procedure we apply here leads to a more confident error margin.

As mentioned before, the background concentration, c_{back} of $1.5 \text{ ng}/\text{m}^3$ used until now is a lower bound for the background concentration that leads to an upper bound estimate for the true GEM emissions. By using $1.8 \text{ ng}/\text{m}^3$ as background concentration (+20%), which is equal to the median and a high estimate for the background, we are able to set a lower bound for emissions. These two margins are more helpful in the error characterization than a technical error propagation approach. Following this approach we obtain a lower bound emission of $2.8 \pm 1.0 \text{ g}/\text{hour}$ (Table 1, mean of the lower bound scenarios of the nine periods \pm standard deviation) and can thereby narrow down the true GEM emissions for Zurich. According to our findings they must amount to a value between 2.8 ± 1.0 and $4.7 \pm 0.9 \text{ g}/\text{hour}$. In this range we also see the sensitivity of the background concentration for the model results. As shown a change in c_{back} by 20% resulted in a mean emission estimate for all nine periods lower by 40%. The sensitivity ($S = (\Delta O/O)/(\Delta I/I)$, MacLeod et al. (2002)) of c_{back} (I) regarding the mean emission estimate (O) amounts to $S = 2$.

After the background concentration, the BLH ~~ist~~ is the most sensitive parameter. An increase of the BLH by 10% results in an equally larger emission estimate, S for the BLH equals 1. As mentioned before the height of 150 m for Zurich has been established in previous model studies from temperature profiles. To test this value and the assumption of a constant height we established an advanced model scenario, where the BLH is derived from a complex numerical weather prediction model COSMO-2, developed by MeteoSchweiz. The BLH is determined both for day and night with an hourly time resolution. The approach for the advanced scenario is presented in detail in the Supplement. All model runs of the advanced scenario are displayed in the Figures S6-S14. The emission estimates based on this advanced approach ($4.9 \pm 1.7 \text{ g}/\text{hour}$, Table S1) are very close to the basic scenario with the fixed BLH presented here ($4.7 \pm 0.9 \text{ g}/\text{hour}$). ~~The~~ Additionally, the advanced model does often not provide a better model fit as RMSE comparison show in Table S1. On this basis and the accordance in the outcome of the two model approaches, we favor the basic approach with a fixed BLH of 150 ~~mis~~ is therefore justified and to reduce the model complexity we recommend this the basic approach. ~~The reason being that thereby we can reduce model complexity, which is not necessary to adequately describe the situation at hand.~~

Other important model parameters to be discussed here are the model area with a sensitivity of $S = 0.6$ and the wind speed $S = 0.4$. If we again look at a steady state example ($\frac{dm}{dt} = 0$) of equation 2 and rearrange to $c = c_{\text{back}} + E/(u \cdot A_s)$, we see that the ratio between the emission flux E and the advective flux ($u \cdot A_s$) is determining the deviation of the concentration from the background concentration $c - c_{\text{back}}$. During the day, advective fluxes are much larger than the emission term we estimate for Zurich. For the small box in Zurich even for very low wind speeds of 1 m/s, F_{adv} is 7 times bigger than E .

Therefore, c is dominated by c_{back} during the day in our model. The explanatory power of the model is much stronger during the nocturnal inversion periods with low BLH and low wind speeds. During these periods advection has little influence. The model application domain for the two cases of high and low BLH are displayed in Figure S18. These curves set the domain regarding the GEM concentrations explainable by our model depending on the BLH, the wind speed and the model area. The model area has to be chosen to encompass all important sources and big enough such as to allow for a reasonable time step in the model set up. For large model areas, however, inhomogeneities in the model region could be problematic. Here, we assume homogeneous distribution of GEM in our model region of 10 km by 10 km. As work by Cairns et al. (2011) shows, GEM concentrations in Toronto do follow a certain distribution and differences in concentrations do occur depending on the measurement location. Our measurement site has been assessed for pollutants with diffuse emissions with passive samplers by comparing various sites throughout the city. The location proved to be a representative study site for an anthropogenic pollutant with diffuse emissions (Diefenbacher et al., 2015b, 2016). As mentioned before mercury emissions in Zurich stem from diffuse sources, which are distributed in the whole city and a waste incineration plant in the city center. Emission estimates derived with our box model only apply to the whole city or can be averaged by person. Spatially resolved emission estimates are, however, not attainable.

Regarding the consistency of the emissions we see from the comparison of the GEM measurements to CO and CH₄ levels (see Fig. 2, S4 and S5) in Zurich emissions largely stem from constant sources. Activity related emissions, i.e. from traffic, are a minor contributor. Also from the comparison between summer and winter periods, which are comparable in terms of emission strength, we conclude that the increased combustion activities during the cold winter months are not a large contributor to overall GEM emissions. Possibly, increased GEM emissions from enhanced combustion activities in winter are compensated by reduced emissions of GEM by evaporation from legacy mercury reservoirs in periods with low ambient temperatures and vice versa in winter.

3.3 Implication on emission reporting

Mercury emissions are annually reported by countries signatories of the Protocol on Heavy Metals to the UNECE Convention on Long-Range Transboundary Air Pollution (CLRTP). Swiss national CLRTP inventories for mercury emissions to the atmosphere reported a total of 658 kg/a for the year 2014 (Heldstab et al., 2015). Mercury emissions are not differentiated by species GEM or GOM. Due to the lack of these data we are forced to work with assumptions. Considering the nature of emission sources and relatively strict regulation on stack emissions we assume all emissions to be in the form of GEM. The biggest share, 73% of the emissions, stems from the energy sector (1A1), of which the majority is allocated to energy industries for public electricity and heat production. Main sources to this energy sector are waste incineration plants. In Switzerland energy recovery from municipal solid waste incineration is mandatory and emissions from waste incineration plants are reported under this category. Other combustion processes mainly in manufacturing industries (1A2:5) make up for 25% of the total emissions. These numbers and categorization into individual sectors and subcategories as shown in Table 2 and set the basis for the allocation to the global emission grid of EMEP for Switzerland. The grid shows spatial resolved emissions with a $0.1^\circ \times 0.1^\circ$ (approx. 10 km \times 10 km) resolution. The allocation rules for the emissions rely mostly on population density

and vary from one to another source category. Depending on the source category, different weightings on the prevailing employment sectors are installed. For Zurich, the gridded emission report an emission flux of 18 kg for the year 2014 (18 kg for 2015). Our boundary-layer budget approach results in a GEM emission flux between 24 and 41 kg for Zurich. These findings suggest emission of about double the amount allocated to Zurich by the rule set for the EMEP report. If we would apply the same allocation factors to the model results we would come up with national GEM emission of 934 to 1581 kg/a, i.e. clearly higher than reported by the authorities. When we use population data only as a criterion, a scaling factor of 20.5 would be appropriate, considering a population of approximately 400'000 residence in the modeled area and a Swiss population of 8.2 million people. This approach would amount to emission of 494 to 837 kg GEM per year. In comparison to the 658 kg/a of the Swiss CLRTP report, these results lie in a very acceptable range and show that the approach explained here can be used to validate national reporting. Moreover, from our results we suggest that the allocation formula for mercury for the EMEP grid should be adjusted such that population data is given more weight over other parameters. For Zurich we find a per capita emission of 0.06 to 0.10 g/a per person. This estimate is somewhat lower than the European per capita emission of 0.19 g/a reported in the AMAP/UNEP (2013) background report.

4 General applicability and conclusions

The boundary-layer approach presented here is based on atmospheric inversion. This phenomenon, however, is not unique only to Zurich, but can be applied to a wide range of cities and industrial complexes of different size all over the world. Diurnal variability with higher nighttime GEM concentrations has for example been observed in Southern England (Lee et al., 1998); Seoul, Korea (Kim and Kim, 2001); Guiyang, China (Feng et al., 2004), and Beijing and Guangzhou, China (Wang et al., 2007). By adapting the model to the localities, emission estimates are feasible and can support authorities in the set-up and improvement of emission inventories. Indicators for inversion are manifold and are manifest by temperature inversion, increases in pollution levels or morning fog. The adaptiveness of the box model approach is displayed in Fig. 4. It shows a graphical representation of the steady-state equation for the emissions ($E = u \cdot A_s \cdot (c - c_{\text{back}})$). We argue that steady-state is reached to a reasonable degree when atmospheric conditions are stable for a period of several hours, depending though on the size of the box and the wind speed. The nomogram (Fig. 4) can be used in order to quickly estimate the emission strength of a city under the assumption of steady-state and well mixed conditions. Two exemplary cities, Beijing, China and Denver, CO, USA of different size are shown in the graph together with Zurich. All of them are located in a valley, a beneficial characteristic but not a requirement to the model. The starting point to read the graph marks the wind speed measured during an inversion period on the bottom right side of the graph. The graph to the left than gives the proportionality between the difference in GEM concentrations of the measurements and the background ($c - c_0$) on the abscissa and the GEM emission strength on the axis of ordinate. A walk through example is given for Beijing with a wind speed of 1.5 m/s. Continuing in a straight path upwards (see gray vertical line on the right part of Fig. 4) the line given by the size of Beijing is reached (black ~~dotted~~-dashed line). The box length for a city and the BLH define the lateral side of the box A_s . Here, we use our standard BLH of 150 m. From this point one draws a horizontal line to the left until the left plot is reached. A GEM concentration difference of 2.6 ng/m³ results in an

emission estimate of 77.5 g/h. Following this example emissions strength of other cities can quickly be estimated according to size of their respective box model, the measured wind speeds and GEM concentrations. The colored lines show the situation in Zurich, i.e. the emission estimations with a wind speed of 0.5 m/s (red lines), 1 m/s (green lines), 2 m/s (blue lines), and 4 m/s (purple line). The distribution of the daily minimum wind speeds and the daily maximum concentration differences measured in Zurich during inversion are given by the density curves at the bottom. These curves set the bandwidths for GEM emissions predicted by the model. The emission estimates of the high and low backgrounds are given by the gray straight lines 2.8 and 4.7 g/hour. The comparison thereof with the emissions from the steady-state box model presented here shows a reasonable accordance.

An other entry point to read the graph is the emissions. For Beijing emission estimates amount to 775 g/h (6.79 t/a) (Streets et al., 2005; Wu et al., 2006; Zhou et al., 2010). Since the formula is all linear both axis of the left graph can as well be multiplied by 10, so the entry is congruent to 77.5 g/h. Concentration difference for a wind speed of 1.5 m/s than amounts to 26 ng/m³ (2.6 ng/m³ × 10), which is a reasonable value for average concentrations in Beijing, considering the GEM measurements reported for the city (4 - 54 ng/m³) (Wang et al., 2007; Zhou et al., 2010). Based on this preliminary assessment a more extensive box model study could be conducted, taking into account specific measurements and as well technical aspects such as the the bigger air compartment, where the inhomogeneities ~~have to been in the air mixing have to be~~ addressed with multiple measurement locations.

For a successful application of this approach, several aspects have to be considered: i) background levels should be stable and not directly influenced by large sources, furthermore the influence of the wind direction has to be assessed ii) the model area has to be chosen wisely, when chosen too large it poses the problem of inhomogeneities in the air compartment; when chosen too small it is dominated too much by advection, depending on wind speed and background GEM levels, iii) the BLH should be stable and some knowledge about the BLH is a prerequisite, best is to check for day/night inversions using an other trace gas such as CO or PM10, v) a closer look at local point sources within the model region is necessary, such as to assess if they pose an overbalance compared to the diffuse emissions; or if their emissions, for example due to high stacks, are actually within the defined model boundaries.

We believe the boundary-layer budget approach presented here is a valuable contribution to the demand for mercury emission inventories by the UN Minamata Convention on Mercury (Article 19, 1.a). The low computational requirements a box model poses and its broad applicability make it a readily available tool that is needed in narrowing down the broader scope of common bottom-up emission estimates. The use of passive samplers for mercury, which allow a cost effective and broad spacial coverage in ambient air monitoring, in combination with box models such as ours pose a great opportunity not only for model refinement, but also for the applicability to other domains. Here, we see great potential of this boundary-layer approach to constrain the emission estimates of diffuse mercury emissions. The fields of application, however, are not limited to mercury alone, other compounds are as well suited for emission estimates by a box model. Furthermore, besides emissions, sinks – a hot topic in mercury research – can also be quantified with the presented boundary-layer budget method.

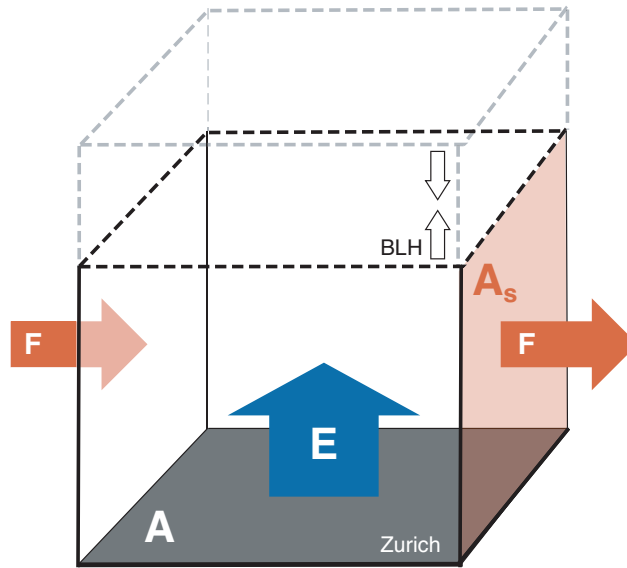


Figure 1. Box model used to estimate GEM emissions E of Zurich. A represents the area of the base and A_s the area of the lateral side of the box. The variable boundary-layer height (BLH) determines the height of the box and F the advective flow.

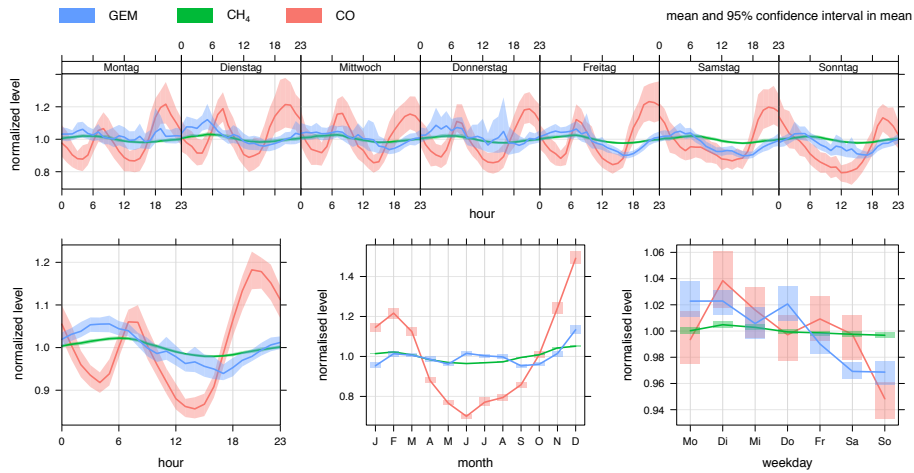


Figure 2. Comparison between normalized GEM, CH_4 and CO levels (divided by overall mean) showing the temporal variation over a weekly, daily, monthly and weekday course. Mean values and 95% confidence intervals are shown. [Source: NABEL (FOEN and Empa) BAFU; EMPA (2018)]

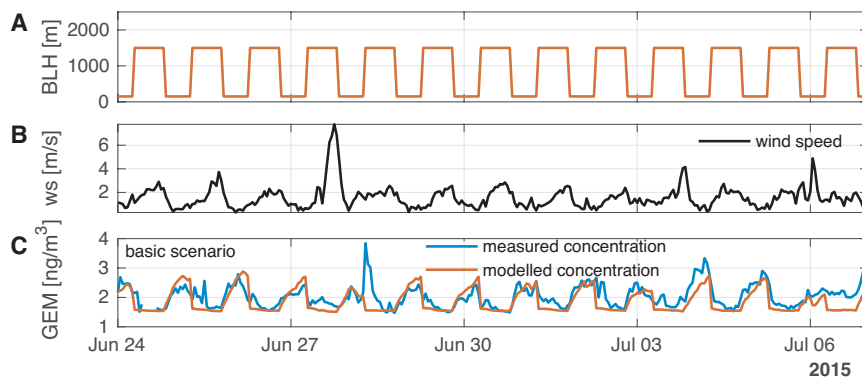


Figure 3. Exemplary period from June 24 until July 06 2015 that shows a day-night pattern for ground inversion. **A** shows the boundary layer heights for both the basic scenario (red). **B** shows the wind speed (ws). **C** shows GEM measurements in blue and the basic model results in red.

Table 1. The emission estimates of GEM in Zurich, Switzerland are shown for all nine observed summer periods.

start	days	emissions [g/hour]	
		upper bound	lower bound
06/06/2014	4	5.7	3.8
16/07/2014	5	4.4	2.5
05/09/2014	4	4.0	2.4
05/03/2015	6	3.5	1.7
18/05/2015	5	3.4	1.1
24/06/2015	14	4.8	3.0
11/07/2015	13	5.9	3.8 3.8
02/08/2015	5	5.7	3.7
28/08/2015	4	4.5	2.7
mean		4.7±0.9	2.8±1
annual [kg/a]		41±8	24±8

Table 2. Swiss national inventory for mercury emissions in 2014 as submitted under the UNECE Convention on Long-range Transboundary Air Pollution. (NFR: nomenclature for reporting emission categories, IPPU: industrial processes and product use)

Hg emissions 2014		national	this study
NFR	category	[kg/a]	[kg/a]
1	power	482	
1A	fuel combustion	482	
A1	energy indust.	279	
A2:5	misc.	162	
2	IPPU	78	
5	waste	35	
6	other	63	
total		658	574 - 951

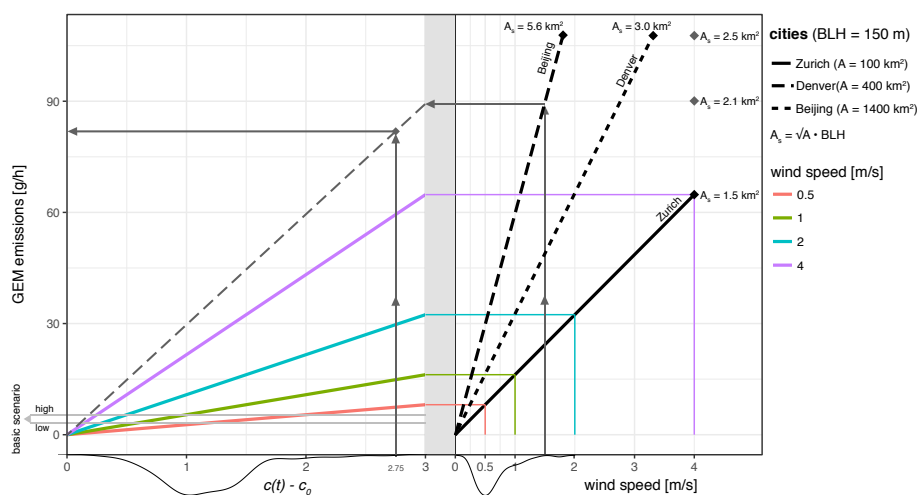


Figure 4. Graphical representation of the steady-state formula $E = u \cdot A_s \cdot (c - c_{\text{back}})$ to estimate emissions in a box model. In color, starting at different windspeed it shows the corresponding GEM emission estimate for Zurich in relation to the concentration difference between measurement c and background c_0 . The results of the basic emission scenario are given as gray lines. The gray shading highlights the range in concentration differences obtained in Zurich. An example how emission are estimated for another city is given for Beijing, with a wind speed of 1.5 m/s and 2.6 ng/m³ concentration difference.

Author contributions. Basil Denzler and Christian Bogdal planned the study and executed the measurements and prepared the manuscript. Cyrill Kern, Anna Tobler and Jing Huo worked on the model development during their masters course. Konrad Hungerbühler supervised the project.

Competing interests. The authors declare that they have no conflict of interest.

- 5 *Acknowledgements.* We would like to thank Stephan Henne (EMPA, Dübendorf) for the helpful advice he provided. Furthermore, we acknowledge the Swiss National Air Pollution Monitoring Network (NABEL) and the Federal Office for Meteorology and Climatology (MeteoSwiss) for providing measurement and meteorological data. We thank the Swiss Federal Office for the Environment (FOEN) for the project funding (grant numbers 00.0248.P2/M371-4632, 14.0039.KP/N412-1043).

References

- AMAP/UNEP: Technical Background Report for the Global Mercury Assessment, Tech. rep., UNEP; AMAP, Geneva; Oslo, 2013.
- BAFU; EMPA: Messergebnisse 2016, Tech. rep., BAFU; EMPA, Bern, 2018.
- Benz, U.: Parametrisierung der planetaren Grenzschichthöhe über der Stadt Zürich, Ph.D. thesis, ETH Zürich, 1988.
- 5 Bogdal, C., Müller, C. E., Buser, A. M., Wang, Z., Scheringer, M., Gerecke, A. C., Schmid, P., Zennegg, M., Macleod, M., and Hungerbühler, K.: Emissions of polychlorinated biphenyls, polychlorinated dibenzo-p-dioxins, and polychlorinated dibenzofurans during 2010 and 2011 in Zurich, Switzerland, *Environmental Science and Technology*, 48, 482–490, <https://doi.org/10.1021/es4044352>, 2014a.
- Bogdal, C., Wang, Z., Buser, A. M., Scheringer, M., Gerecke, A. C., Schmid, P., Müller, C. E., MacLeod, M., and Hungerbühler, K.: Emissions of polybrominated diphenyl ethers (PBDEs) in Zurich, Switzerland, determined by a combination of measurements and modeling, *Chemosphere*, 116, 15–23, <https://doi.org/10.1016/j.chemosphere.2013.12.098>, 2014b.
- 10 Buchmann, B., Stemmler, K., and Reimann, S.: Regional emissions of anthropogenic halocarbons derived from continuous measurements of ambient air in Switzerland, *CHIMIA International Journal for Chemistry*, 57, 522–528, <https://doi.org/10.2533/000942903777678966>, 2003.
- Buser, A. M., Kierkegaard, A., Bogdal, C., Macleod, M., Scheringer, M., and Hungerbühler, K.: Concentrations in ambient air and emissions of cyclic volatile methylsiloxanes in Zurich, Switzerland, *Environmental Science and Technology*, 47, 7045–7051, <https://doi.org/10.1021/es3046586>, 2013.
- 15 Buser, A. M., Bogdal, C., MacLeod, M., and Scheringer, M.: Emissions of decamethylcyclopentasiloxane from Chicago, *Chemosphere*, 107, 473–475, <https://doi.org/10.1016/j.chemosphere.2013.12.034>, 2014.
- Cairns, E., Tharumakulasingam, K., Athar, M., Yousaf, M., Cheng, I., Huang, Y., Lu, J., and Yap, D.: Source, concentration, and distribution of elemental mercury in the atmosphere in Toronto, Canada, *Environmental Pollution*, 159, 2003–2008, <https://doi.org/10.1016/j.envpol.2010.12.006>, 2011.
- 20 Denmead, O. T., Raupach, M. R., Dunin, F. X., Cleugh, H. A., and Leuning, R.: Boundary layer budgets for regional estimates of scalar fluxes, *Global Change Biology*, 2, 255–264, <https://doi.org/10.1111/j.1365-2486.1996.tb00077.x>, 1996.
- Diefenbacher, P. S., Bogdal, C., Gerecke, A. C., Glüge, J., Schmid, P., Scheringer, M., and Hungerbühler, K.: Emissions of Polychlorinated Biphenyls in Switzerland: A Combination of Long-Term Measurements and Modeling, *Environmental Science & Technology*, 49, 2199–2206, <https://doi.org/10.1021/es505242d>, 2015a.
- 25 Diefenbacher, P. S., Bogdal, C., Gerecke, A. C., Glüge, J., Schmid, P., Scheringer, M., and Hungerbühler, K.: Short-Chain Chlorinated Paraffins in Zurich, Switzerland - Atmospheric Concentrations and Emissions, *Environmental Science & Technology*, 49, 9778–9786, <https://doi.org/10.1021/acs.est.5b02153>, 2015b.
- 30 Diefenbacher, P. S., Gerecke, A. C., Bogdal, C., and Hungerbühler, K.: Spatial Distribution of Atmospheric PCBs in Zurich, Switzerland: Do Joint Sealants Still Matter?, *Environmental Science and Technology*, 50, 232–239, <https://doi.org/10.1021/acs.est.5b04626>, 2016.
- Feng, X. B., Shang, L. H., Wang, S. F., Tang, S. L., and Zheng, W.: Temporal variation of total gaseous mercury in the air of Guiyang, China, *Journal of Geophysical Research-Atmospheres*, 109, 1–9, <https://doi.org/10.1029/2003JD004159>, 2004.
- Gasic, B., Moecke, C., Macleod, M., Brunner, J., Scheringer, M., Jones, K. C., and Hungerbühler, K.: Measuring and modeling short-term variability of PCBs in air and characterization of urban source strength in Zurich, Switzerland, *Environmental Science and Technology*, 43, 769–776, <https://doi.org/10.1021/es8023435>, 2009.
- 35

- Gasic, B., MacLeod, M., Klanova, J., Scheringer, M., Ilic, P., Lammel, G., Pajovic, A., Breivik, K., Holoubek, I., and Hungerbühler, K.: Quantification of sources of PCBs to the atmosphere in urban areas: A comparison of cities in North America, Western Europe and former Yugoslavia, *Environmental Pollution*, 158, 3230–3235, <https://doi.org/10.1016/j.envpol.2010.07.011>, 2010.
- Gay, D. A., Schmeltz, D., Prestbo, E., Olson, M., Sharac, T., and Tordon, R.: The Atmospheric Mercury Network: measurement and initial examination of an ongoing atmospheric mercury record across North America, *Atmospheric Chemistry and Physics*, 13, 11 339–11 349, <https://doi.org/10.5194/acp-13-11339-2013>, <http://www.atmos-chem-phys.net/13/11339/2013/>, 2013.
- Hasenfratz, D., Saukh, O., Walser, C., Hueglin, C., Fierz, M., Arn, T., Beutel, J., and Thiele, L.: Deriving high-resolution urban air pollution maps using mobile sensor nodes, *Pervasive and Mobile Computing*, 16, 268–285, <https://doi.org/10.1016/j.pmcj.2014.11.008>, 2015.
- Heldstab, J., Herren, M., and Walder, J.: Switzerland’s Informative Inventory Report 2015, Submission under the UNECE Convention on Long-range Transboundary Air Pollution, Tech. rep., FOEN, Bern, 2015.
- Kim, K. H. and Kim, M. Y.: The temporal distribution characteristics of total gaseous mercury at an urban monitoring site in Seoul during 1999–2000, *Atmospheric Environment*, 35, 4253–4263, [https://doi.org/10.1016/S1352-2310\(01\)00214-X](https://doi.org/10.1016/S1352-2310(01)00214-X), 2001.
- Lee, D. S., Dollard, G. J., and Pepler, S.: Gas-phase mercury in the atmosphere of the United Kingdom, *Atmospheric Environment*, 32, 855–864, [https://doi.org/10.1016/S1352-2310\(97\)00316-6](https://doi.org/10.1016/S1352-2310(97)00316-6), 1998.
- Lowry, D., Holmes, C. W., Rata, N. D., O’Brien, P., and Nisbet, E. G.: London methane emissions: Use of diurnal changes in concentration and $\delta^{13}\text{C}$ to identify urban sources and verify inventories, *Journal of Geophysical Research: Atmospheres*, 106, 7427–7448, <https://doi.org/10.1029/2000JD900601>, 2001.
- MacLeod, M., Fraser, A. J., and Mackay, D.: Evaluating and expressing the propagation of uncertainty in chemical fate and bioaccumulation models., *Environmental toxicology and chemistry*, 21, 700–709, <https://doi.org/10.1002/etc.5620210403>, 2002.
- MacLeod, M., Scheringer, M., Podey, H., Jones, K. C., and Hungerbühler, K.: The origin and significance of short-term variability of semivolatile contaminants in air, *Environmental Science and Technology*, 41, 3249–3253, <https://doi.org/10.1021/es062135w>, 2007.
- Mueller, M. D., Wagner, M., Barmadimos, I., and Hueglin, C.: Two-week NO₂ maps for the City of Zurich, Switzerland, derived by statistical modelling utilizing data from a routine passive diffusion sampler network, *Atmospheric Environment*, 106, 1–10, <https://doi.org/10.1016/j.atmosenv.2015.01.049>, 2015.
- Mueller, M. D., Hasenfratz, D., Saukh, O., Fierz, M., and Hueglin, C.: Statistical modelling of particle number concentration in Zurich at high spatio-temporal resolution utilizing data from a mobile sensor network, *Atmospheric Environment*, 126, 171–181, <https://doi.org/10.1016/j.atmosenv.2015.11.033>, 2016.
- Müller, C. E., Gerecke, A. C., Bogdal, C., Wang, Z., Scheringer, M., and Hungerbühler, K.: Atmospheric fate of poly- and perfluorinated alkyl substances (PFASs): I. Day-night patterns of air concentrations in summer in Zurich, Switzerland, *Environmental Pollution*, 169, 196–203, <https://doi.org/10.1016/j.envpol.2012.04.010>, 2012.
- Nisbet, E. and Weiss, R.: Atmospheric science. Top-down versus bottom-up., *Science (New York, N.Y.)*, 328, 1241–3, <https://doi.org/10.1126/science.1189936>, 2010.
- Richardson, H., Basu, S., and Holtslag, a. a. M.: Improving Stable Boundary-Layer Height Estimation Using a Stability-Dependent Critical Bulk Richardson Number, *Boundary-Layer Meteorology*, 148, 93–109, <https://doi.org/10.1007/s10546-013-9812-3>, 2013.
- Salmond, J. A.: Wavelet analysis of intermittent turbulence in a very stable nocturnal boundary layer: Implications for the vertical mixing of ozone, *Boundary-Layer Meteorology*, 114, 463–488, <https://doi.org/10.1007/s10546-004-2422-3>, 2005.
- Schuhmacher, P.: No Title Messung und numerische Modellierung des Windfeldes über einer Stadt in komplexer Topographie, Ph.D. thesis, ETH Zürich, <https://doi.org/https://doi.org/10.3929/ethz-a-000599817>, 1992.

- Streets, D. G., Hao, J., Wu, Y., Jiang, J., Chan, M., Tian, H., and Feng, X.: Anthropogenic mercury emissions in China, *Atmospheric Environment*, 39, 7789–7806, <https://doi.org/10.1016/j.atmosenv.2005.08.029>, 2005.
- Stull, R. B.: Mean Boundary Layer Characteristics, in: *An Introduction to Boundary Layer Meteorology*, pp. 1–27, Springer Netherlands, Dordrecht, https://doi.org/10.1007/978-94-009-3027-8_1, 1988.
- 5 Szintai, B. and Kaufmann, P.: TKE as a Measure of Turbulence, Tech. Rep. 8, MeteoSwiss, Zurich, 2008.
- van Velzen, D., Langenkamp, H., and Herb, G.: Review: Mercury in waste incineration, *Waste Management & Research*, 20, 556–568, <https://doi.org/10.1177/0734242X0202000610>, 2002.
- Vogelezang, D. H. P. and Holtslag, A. A. M.: Evaluation and model impacts of alternative boundary-layer height formulations, *Boundary-Layer Meteorology*, 81, 245–269, <https://doi.org/10.1007/BF02430331>, 1996.
- 10 Wang, Z., Scheringer, M., MacLeod, M., Bogdal, C., Müller, C. E., Gerecke, A. C., and Hungerbühler, K.: Atmospheric fate of poly- and perfluorinated alkyl substances (PFASs): II. Emission source strength in summer in Zurich, Switzerland, *Environmental Pollution*, 169, 204–209, <https://doi.org/10.1016/j.envpol.2012.03.037>, 2012.
- Wang, Z.-w., Chen, Z.-s., Duan, N., and Zhang, X.-s.: Gaseous elemental mercury concentration in atmosphere at urban and remote sites in China, *Journal of Environmental Sciences*, 19, 176–180, [https://doi.org/10.1016/S1001-0742\(07\)60028-X](https://doi.org/10.1016/S1001-0742(07)60028-X), 2007.
- 15 Wetzel, P. J.: Toward Parameterization of the Stable Boundary Layer, *Journal of Applied Meteorology*, 21, 7–13, [https://doi.org/10.1175/1520-0450\(1982\)021<0007:TPOTSB>2.0.CO;2](https://doi.org/10.1175/1520-0450(1982)021<0007:TPOTSB>2.0.CO;2), 1982.
- Wilson, S. J., Steenhuisen, F., Pacyna, J. M., and Pacyna, E. G.: Mapping the spatial distribution of global anthropogenic mercury atmospheric emission inventories, *Atmospheric Environment*, 40, 4621–4632, <https://doi.org/10.1016/j.atmosenv.2006.03.042>, 2006.
- Wu, Y., Wang, S., Streets, D. G., Hao, J., Chan, M., and Jiang, J.: Trends in anthropogenic mercury emissions in China from 1995 to 2003, *Environmental Science & Technology*, 40, 5312–5318, <https://doi.org/10.1021/es060406x>, 2006.
- 20 Zhang, L., Wang, S., Wu, Q., Wang, F., Lin, C. J., Zhang, L., Hui, M., Yang, M., Su, H., and Hao, J.: Mercury transformation and speciation in flue gases from anthropogenic emission sources: A critical review, *Atmospheric Chemistry and Physics*, 16, 2417–2433, <https://doi.org/10.5194/acp-16-2417-2016>, www.atmos-chem-phys.net/16/2417/2016/, 2016.
- Zhou, X., Du, J., Wang, C., and Liu, S.: Source apportionment and distribution of atmospheric mercury in urban Beijing, China, *Chinese Journal of Geochemistry*, 29, 182–190, <https://doi.org/10.1007/s11631-010-0182-y>, 2010.
- 25 Zinchenko, A. V., Paramonova, N. N., Privalov, V. I., and Reshetnikov, A. I.: Estimation of methane emissions in the St. Petersburg, Russia, region: An atmospheric nocturnal boundary layer budget approach, *Journal of Geophysical Research: Atmospheres*, 107, 4416, <https://doi.org/10.1029/2001JD001369>, 2002.

Boundary-layer investigation

Advanced model set-up

An advanced scenario is designed to focus on the variability of the boundary-layer heights. The goal is to investigate how the basic scenario performs, regarding its assumption of constant NBL and CBL height, in comparison to an advanced scenario with a more lifelike representation of the boundary-layer heights. To accomplish this, we use the data of the COSMO-2 model, a numerical weather model with 2.2 km by 2.2 km resolution from MeteoSchweiz (Swiss Federal Office of Meteorology and Climatology). The heights are obtained by using the bulk Richardson number (Ri_b) as a stability criteria. Ri_b is built by the ratio of production or dissipation of turbulence by buoyancy and the mechanical turbulence through wind shear. It is a widely used stability criteria in numerical weather prediction models (Richardson et al., 2013). A critical threshold value for Ri_b of 0.33 Wetzel (1982) for calculating the height of the NBL and 0.22 (Vogelezang and Holtslag, 1996) for CBL is used. If the Ri_b approach misses to provide a boundary-layer height, it is determined by the vertical gradient of the potential temperature with a critical value of <0.72 K/100 m according to Szintai and Kaufmann (2008).

Advanced scenario

The comparison of the BLH modeled in the two scenarios – e.g. the basic scenario with constant BLH and the advanced scenario with the BLH derived from meteorological models – shows two main differences in Figure 3a. Firstly, the BLH during the day rises higher for the advanced scenario. This, however, does not have a strong influence on the modeled concentration since in both cases modeled concentration do approach background concentrations during the day (Fig. 3d). The second difference concerns the nighttime BLH, which for the advanced scenario forms earlier in the evening and is not as stable. Its height differs between the nights and is often larger than 150 m, especially towards the end of the selected period. This leads to modeled concentrations which do not reach the same levels as the measurements. At times, modeled concentrations for the basic run decline faster than the measurements in the morning. This suggests the transition of the BLH from nocturnal to daytime to be smoother than the step function in the basic scenario. The advanced scenario better accounts for that. With 5.7 g/hour the emission estimate for the advanced method is slightly higher than for the basic scenario during the selected period. In average over all periods, however, with 5.2 g/hour GEM emissions for the advanced scenario are slightly lower than for the basic run. For some periods selected for the characteristic day/night pattern, the estimation of the BLH do not follow the expected trends and no clear day/night inversion is observable. These periods are highlighted in gray in Table S1 and are not included in the evaluation for the advanced method. Considering the additional complexity and the additional data requirements of the advanced method, we clearly favor the basic method to assess the cities source strength. But we can use the alternative estimation of the BLH conducted for this scenario as a valuable validation. The proximity of the two methods regarding the emission estimates supports the way the BLH is set for the basic scenario.

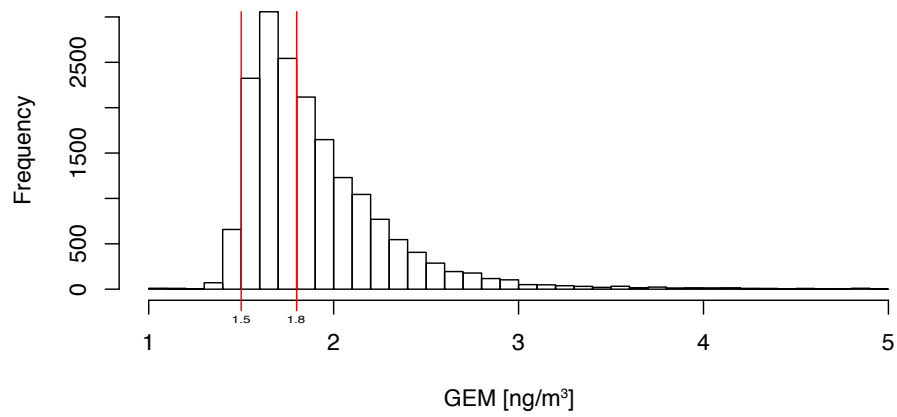


Figure S1. Histogram of GEM concentrations in Zurich from December 2013 until December 2015. Red lines show background levels as they were chosen for the box model.

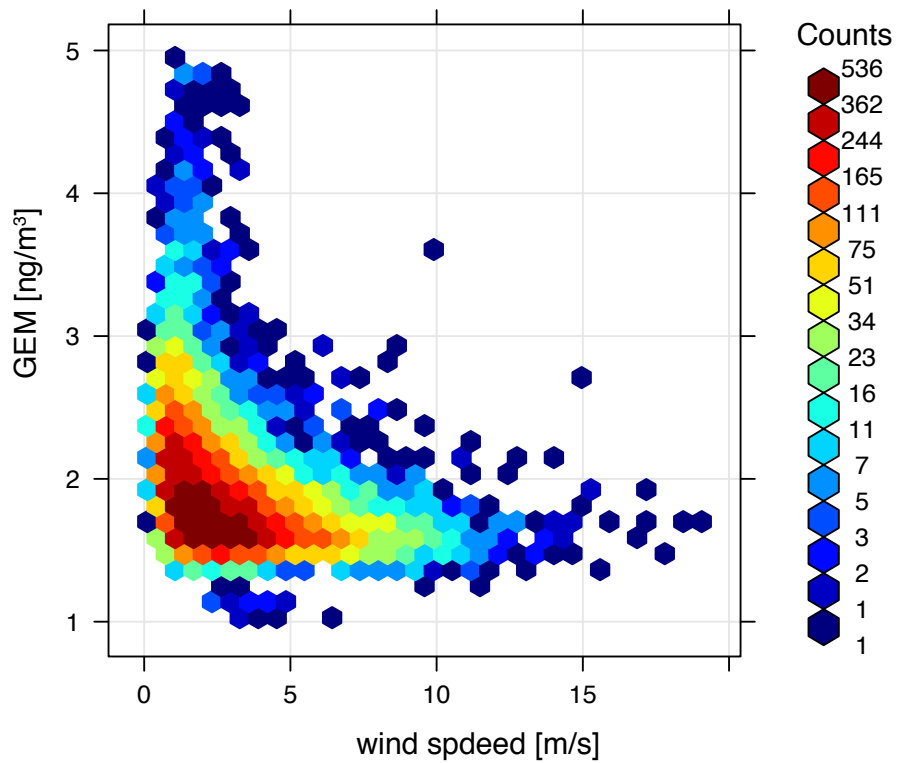


Figure S2. Scatter plot for GEM concentrations and wind speed in Zurich. The tiles represent the number of incidences.

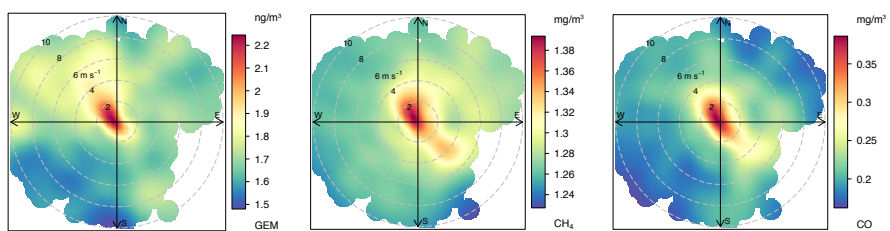


Figure S3. Wind rose plots for GEM, CH₄ and CO concentrations measured in Zurich over the course of 2 years, from December 2013 until December 2015.

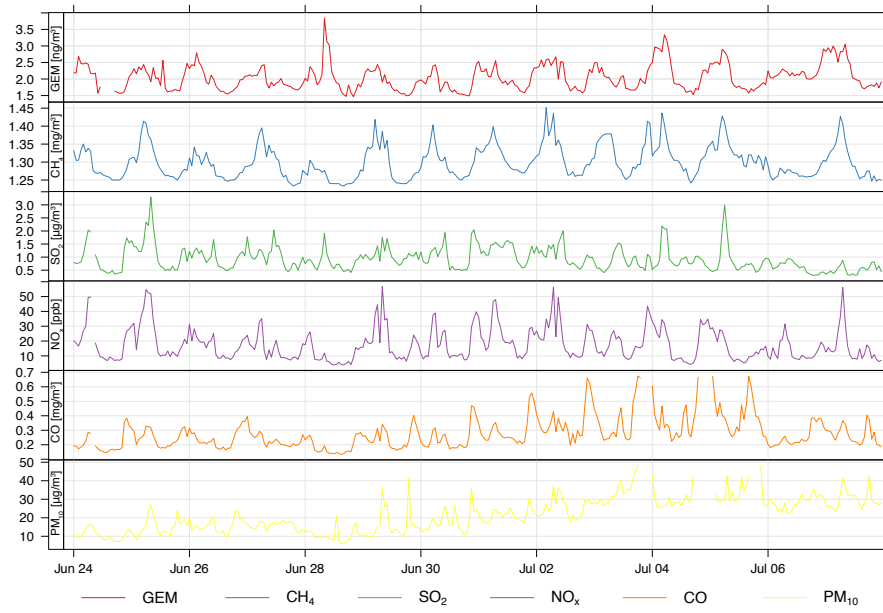


Figure S4. Pollutant measurements for a summer inversion period in Zurich from 24.06.2015 until 7.07.2015.

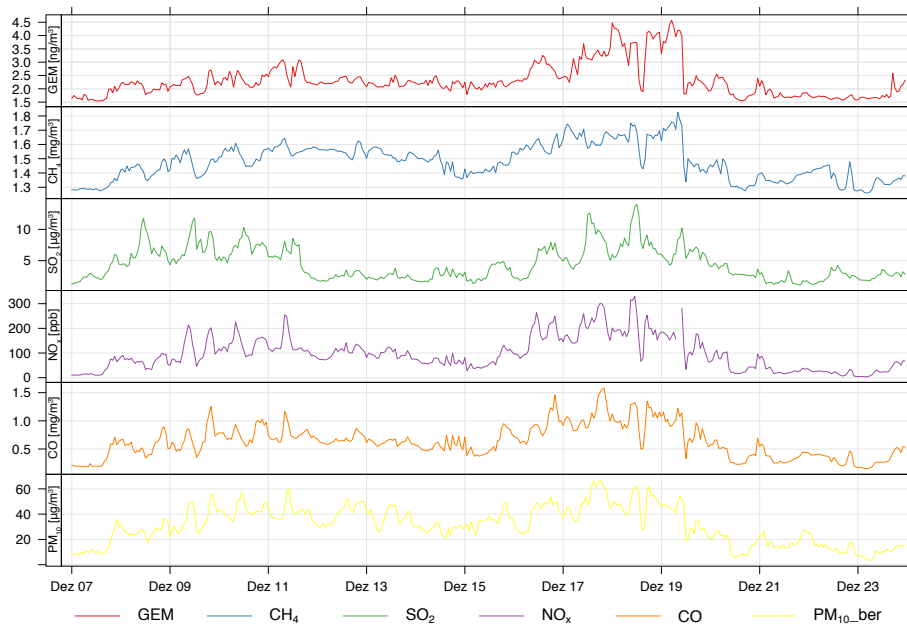


Figure S5. Pollutant measurements for a winter inversion period in Zurich from 07.12.2013 until 24.12..2013.

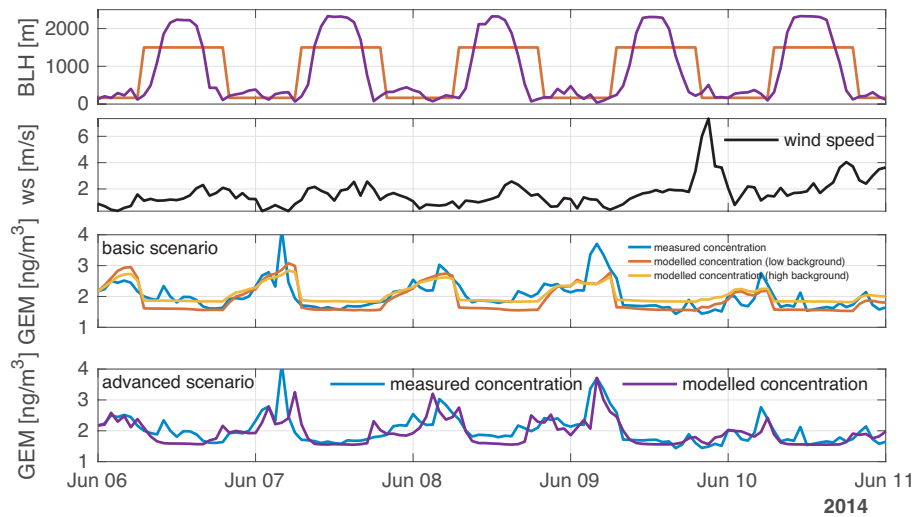


Figure S6. Period with day-night inversion showing the boundary layer height, as approximated in the model; basic scenario (red), advanced scenario (purple). The wind speed (black) is shown in the second plot. The third shows the diurnal pattern for GEM measurements (blue) with the basic scenario model results for high (yellow) and low background (red). The last plot shows the output of the advanced scenario (purple).

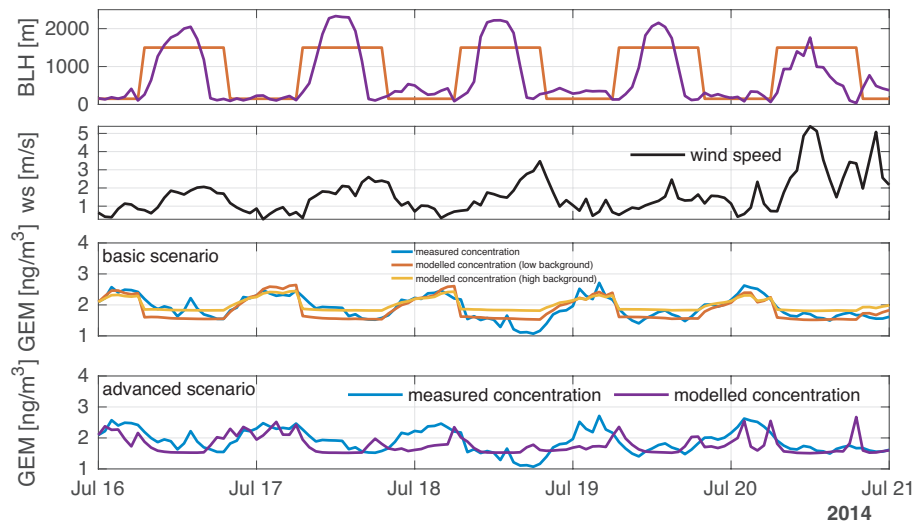


Figure S7. Period with day-night inversion showing the boundary layer height, as approximated in the model; basic scenario (red), advanced scenario (purple). The wind speed (black) is shown in the second plot. The third shows the diurnal pattern for GEM measurements (blue) with the basic scenario model results for high (yellow) and low background (red). The last plot shows the output of the advanced scenario (purple).

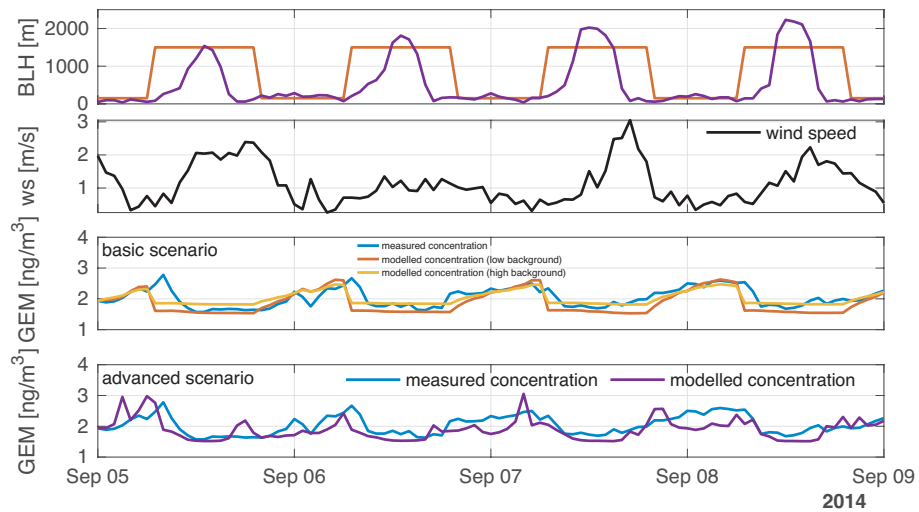


Figure S8. Period with day-night inversion showing the boundary layer height, as approximated in the model; basic scenario (red), advanced scenario (purple). The wind speed (black) is shown in the second plot. The third shows the diurnal pattern for GEM measurements (blue) with the basic scenario model results for high (yellow) and low background (red). The last plot shows the output of the advanced scenario (purple).

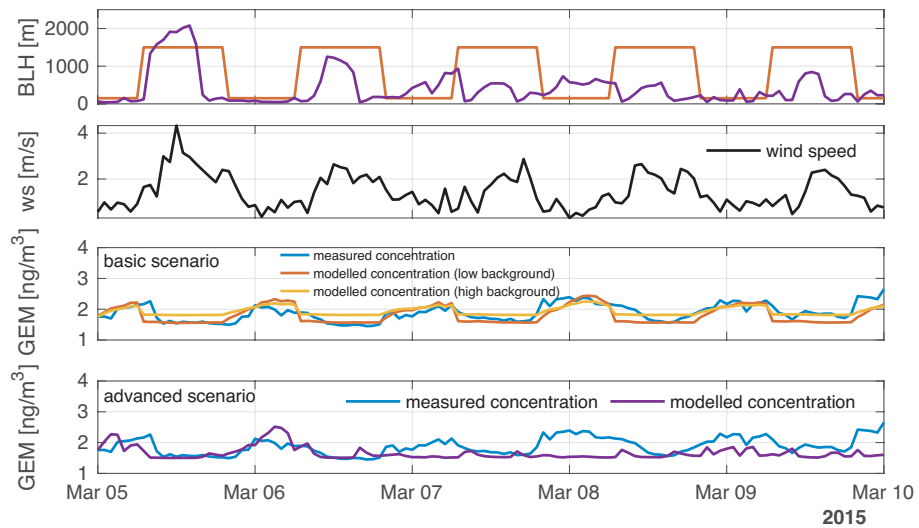


Figure S9. Period with day-night inversion showing the boundary layer height, as approximated in the model; basic scenario (red), advanced scenario (purple). The wind speed (black) is shown in the second plot. The third shows the diurnal pattern for GEM measurements (blue) with the basic scenario model results for high (yellow) and low background (red). The last plot shows the output of the advanced scenario (purple).

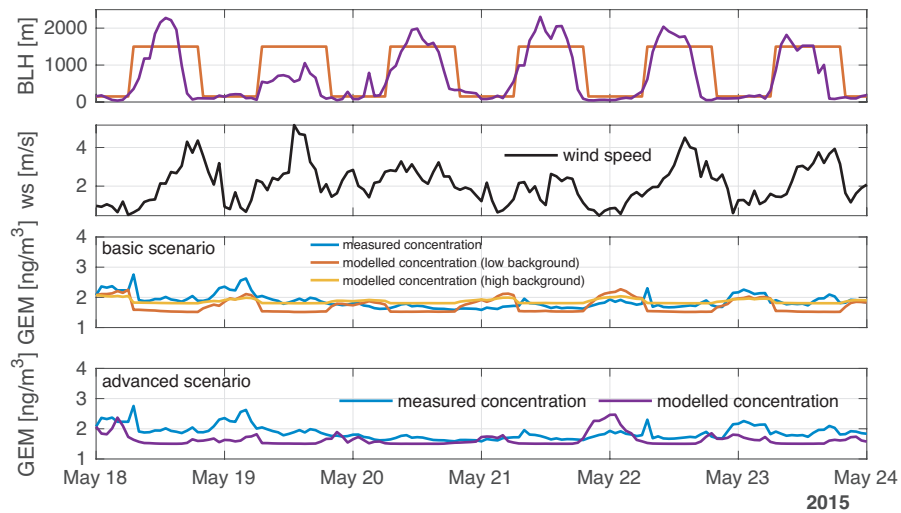


Figure S10. Period with day-night inversion showing the boundary layer height, as approximated in the model; basic scenario (red), advanced scenario (purple). The wind speed (black) is shown in the second plot. The third shows the diurnal pattern for GEM measurements (blue) with the basic scenario model results for high (yellow) and low background (red). The last plot shows the output of the advanced scenario (purple).

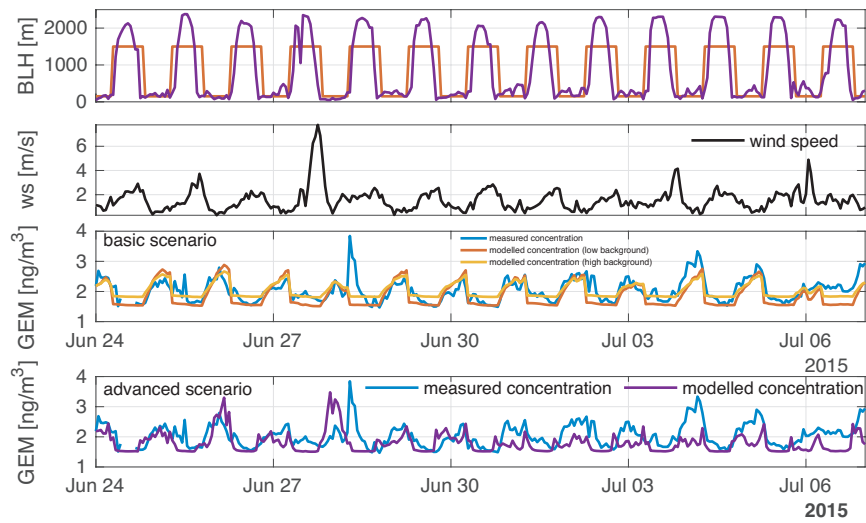


Figure S11. Period with day-night inversion showing the boundary layer height, as approximated in the model; basic scenario (red), advanced scenario (purple). The wind speed (black) is shown in the second plot. The third shows the diurnal pattern for GEM measurements (blue) with the basic scenario model results for high (yellow) and low background (red). The last plot shows the output of the advanced scenario (purple).

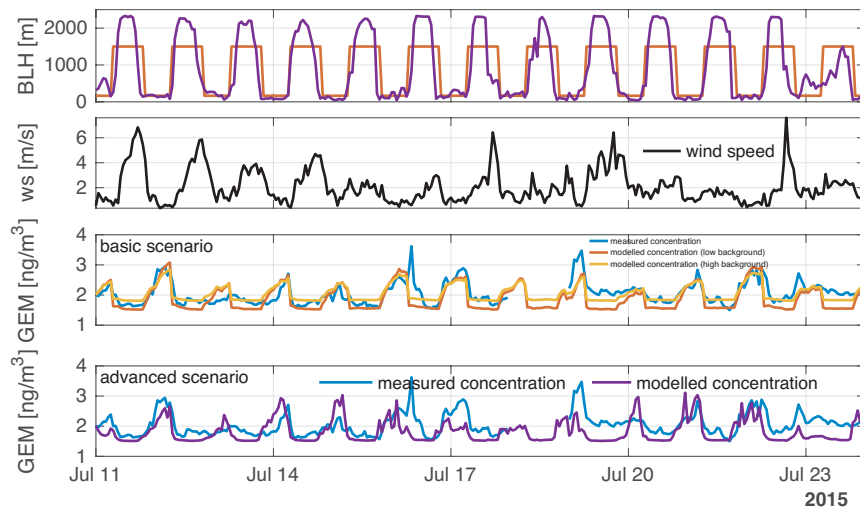


Figure S12. Period with day-night inversion showing the boundary layer height, as approximated in the model; basic scenario (red), advanced scenario (purple). The wind speed (black) is shown in the second plot. The third shows the diurnal pattern for GEM measurements (blue) with the basic scenario model results for high (yellow) and low background (red). The last plot shows the output of the advanced scenario (purple).

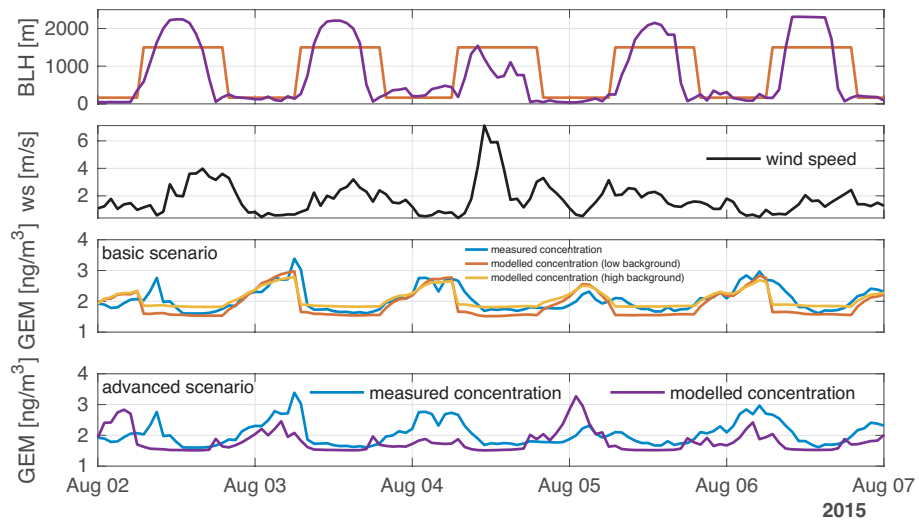


Figure S13. Period with day-night inversion showing the boundary layer height, as approximated in the model; basic scenario (red), advanced scenario (purple). The wind speed (black) is shown in the second plot. The third shows the diurnal pattern for GEM measurements (blue) with the basic scenario model results for high (yellow) and low background (red). The last plot shows the output of the advanced scenario (purple).

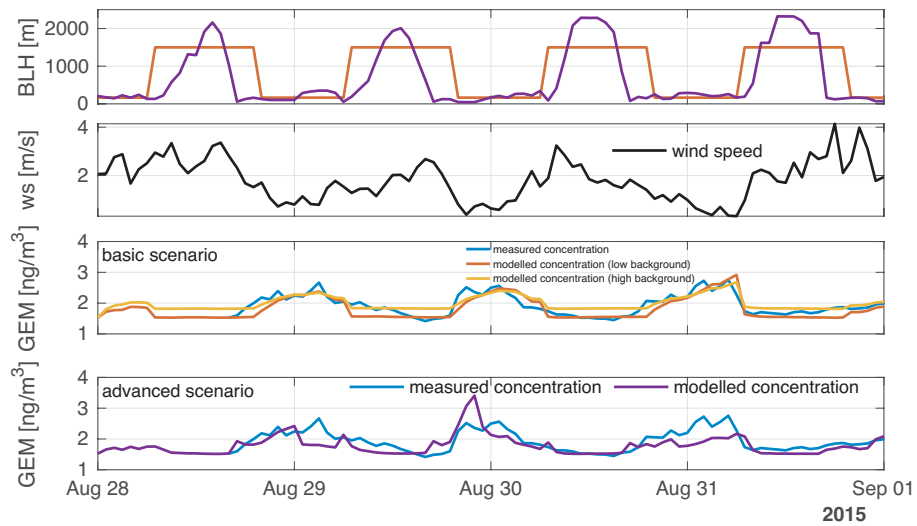


Figure S14. Period with day-night inversion showing the boundary layer height, as approximated in the model; basic scenario (red), advanced scenario (purple). The wind speed (black) is shown in the second plot. The third shows the diurnal pattern for GEM measurements (blue) with the basic scenario model results for high (yellow) and low background (red). The last plot shows the output of the advanced scenario (purple).

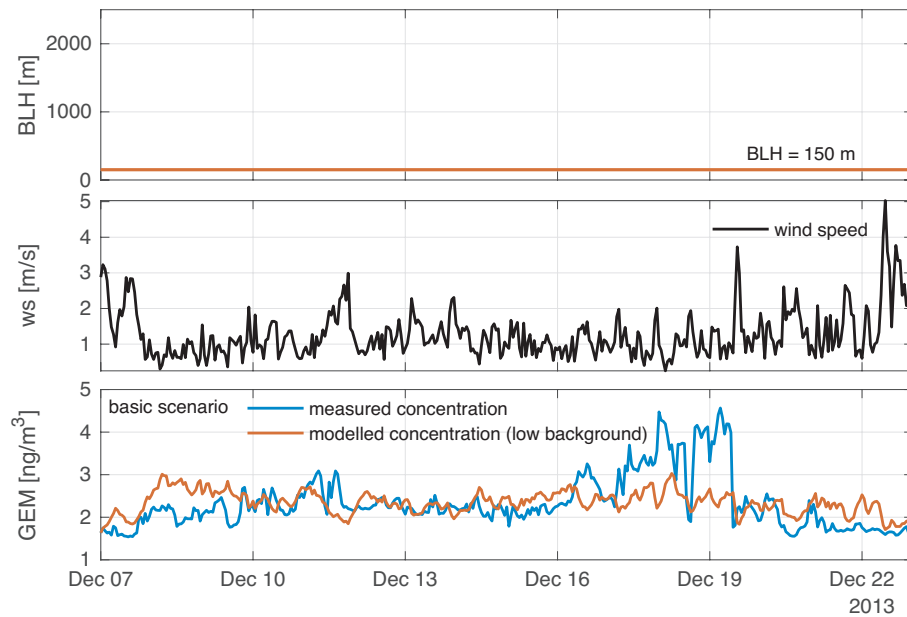


Figure S15. Winter period with stable inversion showing the boundary layer height, as approximated in the model; basic scenario (red), 150 m. The wind speed (black) is shown in the second plot. The third shows the diurnal pattern for GEM measurements (blue) with the basic scenario model results (red).

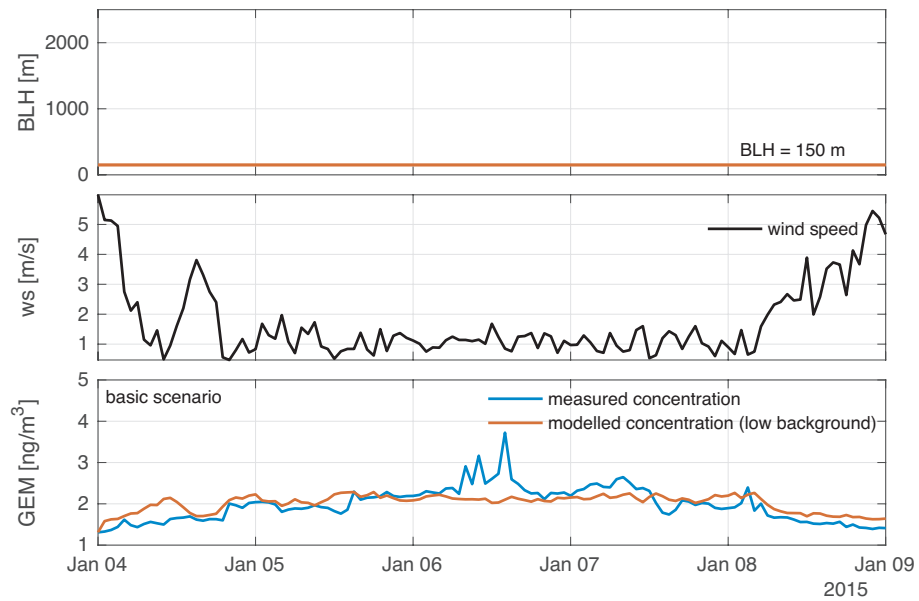


Figure S16. Winter period with stable inversion showing the boundary layer height, as approximated in the model; basic scenario (red), 150 m. The wind speed (black) is shown in the second plot. The third shows the diurnal pattern for GEM measurements (blue) with the basic scenario model results (red).

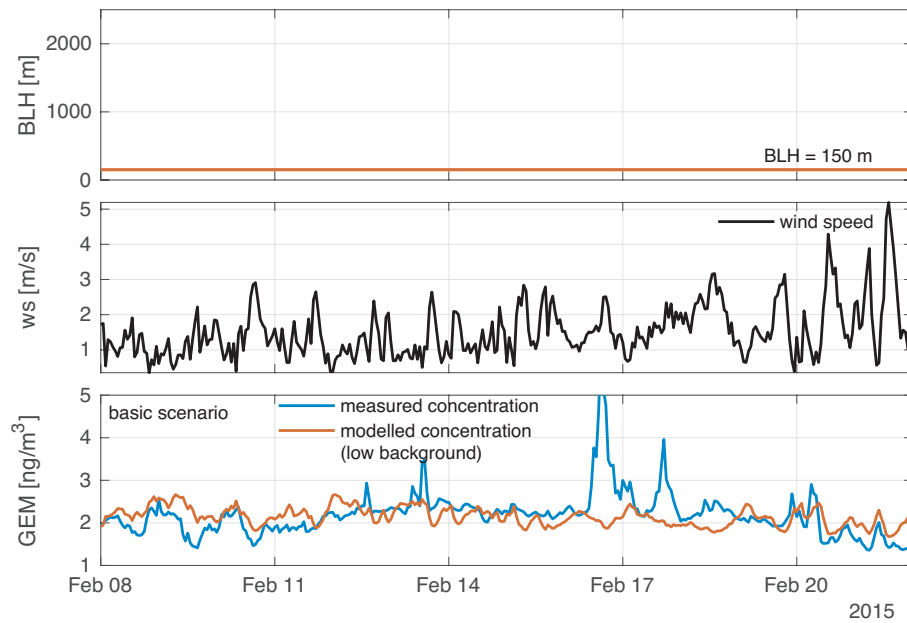


Figure S17. Winter period with stable inversion showing the boundary layer height, as approximated in the model; basic scenario (red), 150 m. The wind speed (black) is shown in the second plot. The third shows the diurnal pattern for GEM measurements (blue) with the basic scenario model results (red).

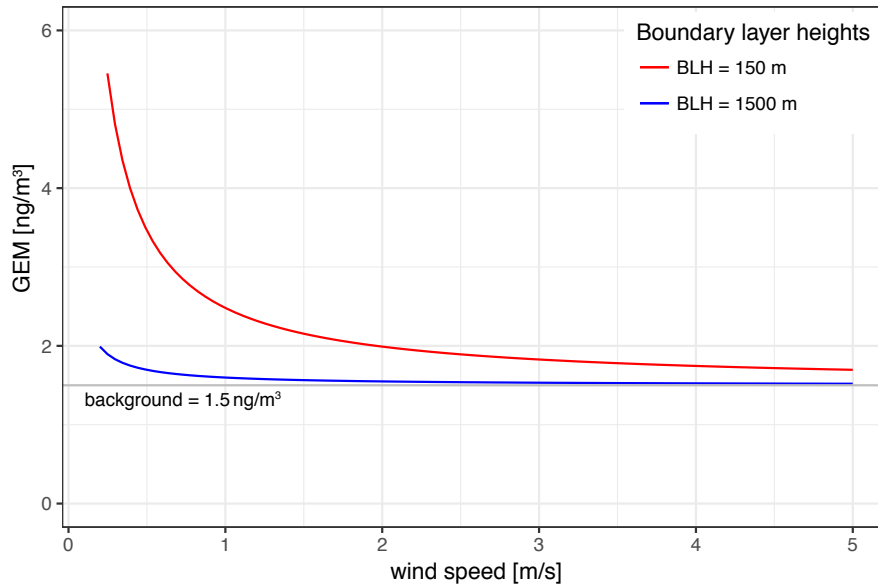


Figure S18. For the steady state assumption $c = c_{\text{back}} + E/(u \cdot A_s)$, GEM concentrations are displayed for the lower air compartment depending on the wind speed once for a boundary layer height of 150 m (red) and for a height of 1500 m (blue). Background concentrations are 1.5 ng/m^3 (gray).

Table S1. The emission estimates of GEM in Zurich, Switzerland are shown for all observed periods. Additionally, the residual mean squares errors (RMSE) for each period and model fit is shown.

start	days	basic scenario				advanced scenario	
		upper bound		lower bound		emissions [g/hour]	RMSE
		emissions [g/hour]	RMSE	emissions [g/hour]	RMSE		
06/06/2014	4	5.7	0.36	3.8	0.33	8.2	0.37
16/07/2014	5	4.4	0.23	2.5	0.25	5.3	0.32
05/09/2014	4	4.0	0.33	2.4	0.23	3.8	0.24
05/03/2015	6	3.5	0.25	1.7	0.22	1.9	0.28
18/05/2015	5	3.4	0.30	1.1	0.21	2.0	0.22
24/06/2015	14	4.8	0.36	3.0	0.29	5.4	0.35
11/07/2015	13	5.9	0.35	3.8	0.27	4.5	0.33
02/08/2015	5	5.7	0.33	3.7	0.27	3.3	0.40
28/08/2015	4	4.5	0.22	2.7	0.20	3.6	0.27
mean		4.7±0.9		2.8±1		4.9±1.7	
annual [kg/a]		41±8		24±8		43±15	
winter							
07/12/2013		5.1		3.4		-	
10/12/2014		3.6		1.8		-	
08/02/2014		4.6		2.6		-	